This is an open access article published under a Creative Commons Attribution (CC-BY) License, which permits unrestricted use, distribution and reproduction in any medium, provided the author and source are cited.

ACS APPLIED ELECTRONIC MATERIALS

pubs.acs.org/acsaelm Article

Photophysics of TADF Guest–Host Systems: Introducing the Idea of Hosting Potential

Kleitos Stavrou, Larissa G. Franca, and Andrew P. Monkman*

Cite This: https://dx.doi.org/10.1021/acsaelm.0c00514 Read Online

ACCESS | Metrics & More | Article Recommendations | Supporting Information

ABSTRACT: The thermally activated delayed fluorescence (TADF) donor–acceptor (D–A) molecule, DMAC–TRZ, is used as a TADF emitter "probe" to distinguish the environmental effects of a range of solid-state host materials in guest–host systems. Using the guest's photophysical behavior in solution as a benchmark, a comprehensive study using a variety of typical TADF organic light-emitting diode hosts with different characteristics provides a clearer understanding of guest–host interactions and what affects emitter performance in solid state. We investigate which are the key host characteristics that directly affect charge-transfer (CT) state energy and singlet triplet energy gaps. Using time-resolved photoluminescence measurements, we use the CT state energy distribution obtained from the full width at half-maximum (fwhm) of the emission band and correlate this with other photophysical properties such as the apparent dynamic red shift of CT emission on-set to estimate the disorder-induced heterogeneity of D–A dihedral angles and singlet triplet gaps. Further, the delayed emission stabilization energy value and time-dependent CT band fwhm are shown to be related to a combination of host's rigidity, emitter molecule packing, and the energy difference between guest and host lowest energy triplet states. Concentration dependence studies show that emitter dimerization/aggregation can improve as well as reduce emission efficiency depending on the characteristics of the host. Two similar host materials, mCPCN and mCBPCN, with optimum host characteristics show completely different behaviors, and their hosting potential is extensively explored. We demonstrate that type I and type III TADF emitters behave differently in the same host and that the materials with intrinsic small ΔE_{ST} have the smallest disorder-induced CT energy and reverse intersystem crossing rate dispersion. We also present an optimized method to define the actual triplet energy of a guest–host system, a crucial parameter in understanding the overall mechanism of the TADF efficiency of the system.

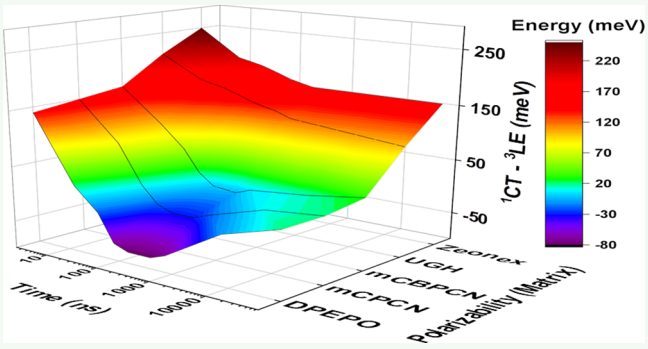

KEYWORDS: *OLED, TADF, organic materials, photophysics, guest–host interactions, packing, homogeneity, polarizability*

Downloaded via 51.194.75.174 on September 3, 2020 at 13:53:54 (UTC).
See https://pubs.acs.org/sharingguidelines for options on how to legitimately share published articles.

■ INTRODUCTION

Development of efficient organic light-emitting diode (OLED) technology[1,2] has been limited by electrical recombination in the active layer, which due to spin statistics forms 25% of singlet states and 75% of triplet states.[3−5] As radiative relaxation from triplet states is forbidden by Pauli's principle,[6] the internal quantum efficiency can achieve a maximum of 25%.[7,8] To overcome this, ways of harvesting triplet states to improve the efficiency of the emission layer of OLEDs have been devised. Two classes of emitter materials, phosphorescent and thermally activated delayed fluorescence (TADF) materials, are playing an important role to harvest 100% of triplet states.[9,10] Phosphorescent materials containing heavy metals, such as platinum[11,12] and iridium,[13] creating strong spin–orbit coupling activate triplet state radiative decay.[14] On the other hand, TADF molecules convert triplet states into an emissive singlet state through thermal activation of a vibronically coupled spin–orbit mechanism given a small energy gap between triplet and singlet states (ΔE_{ST}) and a third state to mediate the exchange.[15−17]

TADF molecules containing donor (D) and acceptor (A) units achieve this *via* charge-transfer (CT) excited states.[18] If the D–A structure leads to effective separation of highest occupied molecular orbital (HOMO) and lowest unoccupied molecular orbital (LUMO), through near-orthogonal D–A relative orientation (typically *via* a C–N bond or spiro bridging bond) the electron-exchange energy is minimized to achieve very small ΔE_{ST}.[2,19,20] ΔE_{ST} below 50 meV enables efficient room-temperature reverse intersystem crossing (rISC)

Received: June 16, 2020
Accepted: August 11, 2020
Published: August 11, 2020

 © XXXX American Chemical Society

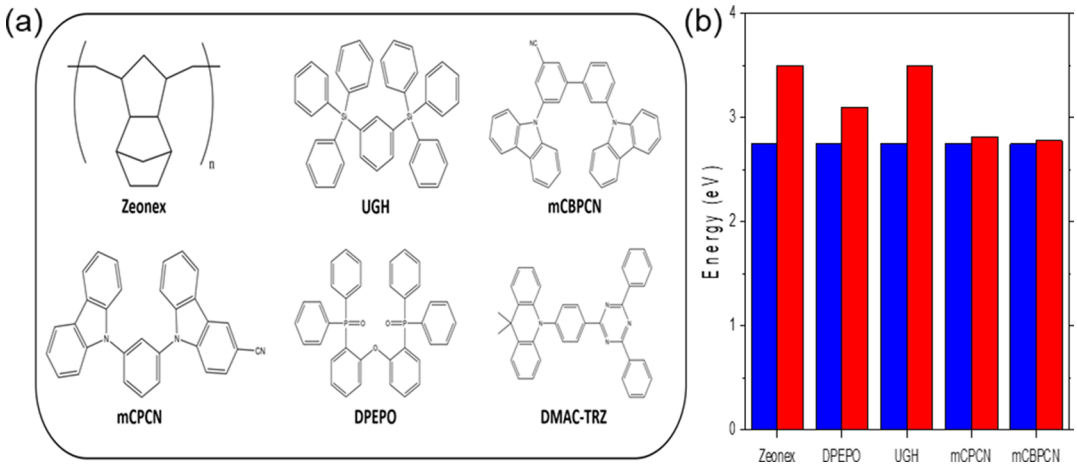

Figure 1. (a) Materials structure and (b) triplet energy values of the different host molecules (red) compared to DMAC−TRZ guest molecules (blue). Note that it is not possible to obtain the triplet energy of Zeonex with the equipment available to the authors, so a hypothetical value is given. Triplet energy of mCPCN and mCBPCN was obtained experimentally in this work (Figure S16), while UGH and DPEPO were found in the literature.[35,42]

between singlet and triplet CT singlet states (^{1}CT and ^{3}CT), given that a localized triplet state (^{3}LE) mediates this process. This requires the ^{3}LE to lie within the same energy range ΔE_{ST} of the ^{1}CT state to vibrationally mix with ^{3}CT, and owing to its different spatial wave functions, the orbital angular momentum can change during a spin flip transition; thus, the ^{3}LE mediates rISC by allowing spin−orbit coupling with the ^{1}CT.[10,21] Once rISC is relatively fast,[22] the process can compete with the nonradiative decay rate,[23] avoiding the energy losses and achieving a high total fluorescence yield (prompt + delayed).[24,25]

In the context of an OLED (emission layer), the emitter is incorporated with one or more host molecules, which not only control the electrical transport properties of the emission layer but also provide a way to avoid self-quenching of the emitter.[26] Emitters tend to aggregate and form dimers and so forth, further sources of nonradiative losses.[27−29] To choose a host molecule for a specific guest emitter, several properties are important, for example, higher energy host triplet state than the emitter, to avoid quenching of the emitter triplet state, which quenches TADF.[30−32] The possibility of host energy transfer to guest and also bipolar charge transport properties must be taken into account in choosing a molecule to act as a host.[33,34]

However, other relevant effects must be considered on the introduction of a host matrix: polarizability and packing. While LE states are not sensitive to the environment, the large dipole moments of CT states readily interact with the host causing changes in energy of this state.[28] By increasing static dielectric coefficient/polarizability of the host, a (static) lowering of the CT state energy can be achieved without affecting the (mediating) LE state energy.[28,35] We note that in a rigid host matrix there cannot be solvatochromism because this requires the rearrangement of the solvent shell so that the permanent dipole moments of the solvent molecules relax the charge-separated state on the solute, increasing the Coulomb attraction energy and therefore lowering the CT energy. As mentioned before, ΔE_{ST} is directly affected by the dihedral angles between the donor and acceptor units, that is, different conformations.[36] In this way, some host molecular structures favor stacking between them, forming a compact matrix. Other structures of the host with more free volume might allow slight motion of the guest in the matrix, leading to the distribution of D−A bridge dihedral angles, thus a distribution of energy CT states.[35,37] Consequently, all these aspects are parameters, which can be optimized for each emitter host combination.

In this study, we investigate the detailed interactions between the host and the guest for a range of different guests to understand how these interactions affect photophysical properties. From this new design, parameters which can further optimize the efficiency of TADF and hence OLED performance are identified. DMAC−TRZ was chosen as the guest, while different hosts were used to compose the matrix. DMAC−TRZ is a well-known TADF emitter, which has 9,9-dimethyl-9,10-dihydroacridine (DMAC) as the electron-donor moiety and 2,4,6-triphenyl-1,3,5-triazine (TRZ) as the electron-acceptor moiety. As the first report of this molecule,[38] DMAC−TRZ presented an efficient TADF mechanism with high photoluminescence quantum yield (PLQY) even in neat films.

■ EXPERIMENTAL SECTION

Sample Preparation. Photophysical characterization of solutions was performed in three different solvents: methylcyclohexane (MCH), toluene, and dichloromethane. All solutions were prepared at a concentration of 20 μM and degassed by five freeze−pump−thaw cycles. Solid-state samples were fabricated by drop-casting and evaporation method onto quartz and transparent sapphire substrates. All host−guest drop-cast films were produced at 1% w/w DMAC−TRZ in a host matrix [Zeonex, DPEPO (bis[2-(diphenylphosphino)-phenyl]ether oxide)], UGH [*m*-bis(triphenylsilyl)benzene], mCPCN [[9-(3-(9*H*-carbazol-9-yl)phenyl)-9*H*carbazole-3-carbonitrile]], and mCBPCN [9-(30-(9*H*-carbazole-9-yl)-5-cyano[1,10-biphenyl]-3-yl)-9*H*-carbazole-3-carbonitrile)]. For neat drop-cast films, a solution of 1 mg/mL was added dropwise onto the substrate. Host−guest evaporated films were made by coevaporation deposition at an evaporation rate of 0.9 Å/s for the host and 0.1 Å/s for DMAC−TRZ materials. For neat evaporated films, the evaporation deposition was performed at a rate of 0.5 Å/s. All evaporated films were prepared using a Kurt J. Lesker Super-Spectros 200 deposition system under vacuum, 10^{-7} mbar, and a final thickness of 100 nm was obtained.

Photophysical Characterization. Steady-state absorption and emission spectra were measured using a double-beam Shimadzu UV-3600 UV/VIS/NIR spectrophotometer and a HORIBA Jobin Yvon Fluorolog-3 spectrofluorometer. Time-resolved measurements were detected by a spectrograph and a gated intensified charge-coupled

https://dx.doi.org/10.1021/acsaelm.0c00514
ACS Appl. Electron. Mater. XXXX, XXX, XXX−XXX

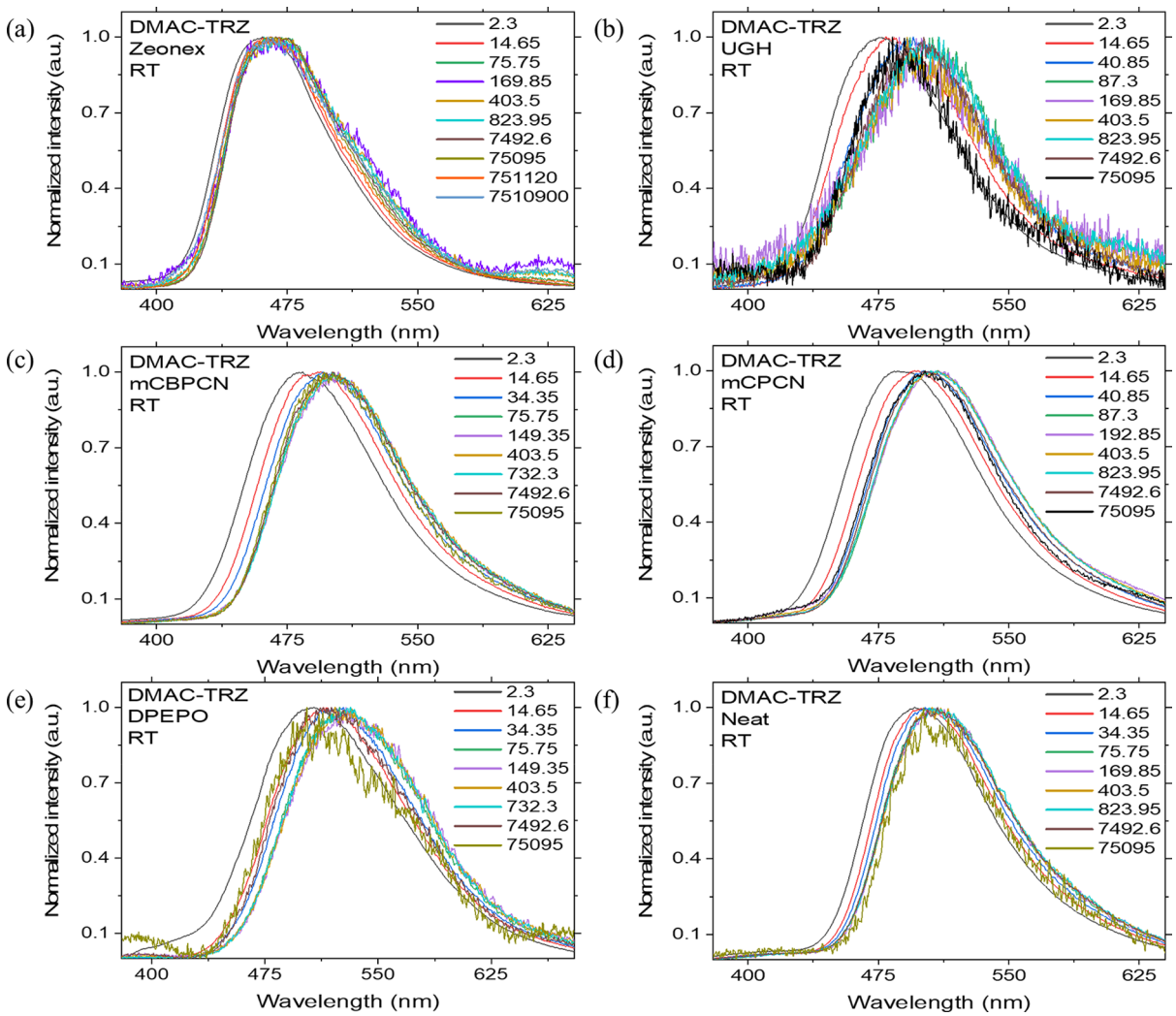

Figure 2. Time-resolved PL spectra, at 298 K (RT), of 1% w/w DMAC−TRZ in (a) Zeonex, (b) UGH, (c) mCBPCN, (d) mCPCN, and (e) DPEPO host. (f) Neat film of DMAC−TRZ. Times given on each plot are in nanoseconds, unless stated.

device (iCCD) camera (Stanford Computer Optics), where samples were excited with a Nd:YAG laser (EKSPLA), 10 Hz, 355 nm or by using a nitrogen laser, 10 Hz, 337 nm, for power dependence measurement. PLQYs were measured using a calibrated integration sphere (HORIBA Quanta-ϕ) coupled to a HORIBA Fluorolog-3 spectrofluorometer. The integration spheres were purged for 30 min in dry nitrogen gas. PLQY values were obtained by exciting at two different wavelengths: 370 and 400 nm.

■ RESULTS AND DISCUSSION

The DMAC−TRZ (Figure 1a) absorption spectra (Figure S1) exhibit two low-energy bands, with peaks at 370 and 410 nm, in MCH, wherein, with increasing solvent polarity, there is a decrease in the oscillator strength and red shift of the 410 nm band around 450 nm, indicative of a direct CT transition. The 370 nm band is unaffected by the solvent (but its intensity decreases because of the loss of the underlying CT transition). An isoemissive point may occur at *ca.* 430 nm. Both transitions have low extinction coefficients (of order 2×10^3 M^{-1} cm^{-1}), from which we can conclude that the second band is from an nπ* transition of the DMAC nitrogen lone pair electrons which are weakly conjugated into the TRZ unit. Previously, we have shown for a phenyl-substituted DMAC−TRZ where the steric hindrance of the phenyl ring causes the DMAC to take a pseudo axial configuration, this greatly increases the conjugation of the nitrogen lone pair into the TRZ unit.[39] In planar, quasi equatorial DMAC−TRZ, this conjugation is much weaker; however, because the energy of the nπ* transition is in close proximity to the direct CT transition, mixing of these two states will increase the oscillator strength of the direct CT transition.[40,41] As polarity is increased and the CT state energy relaxes and red-shifts the CT transition, the mixing of these two states decreases, leading to the strong decrease in the oscillator strength of the CT transition. This local nπ* state could well play a critical role in increasing the oscillator strength of the CT state decay as well, giving rise to the fast radiative decay in weakly polar environments giving rise to the high PLQY of DMAC−TRZ. Photoluminescence (PL) spectra (Figure S1) show a large bathochromic shift in emission with increasing solvent polarity even moderately. In the lower polarity solvent, MCH, well-defined vibronically structured spectra are observed. With increasing polarity, emission spectra red shift and the band becomes structureless and Gaussian band-shaped, a clear indication of a strong low-energy intramolecular CT excited state.

In Figure S2a, we show the time-resolved PL decay of DMAC−TRZ in toluene. There are clearly two decay regimes: the prompt (0−100 ns) and the delayed (0.1−30 μs). The

https://dx.doi.org/10.1021/acsaelm.0c00514
ACS Appl. Electron. Mater. XXXX, XXX, XXX−XXX

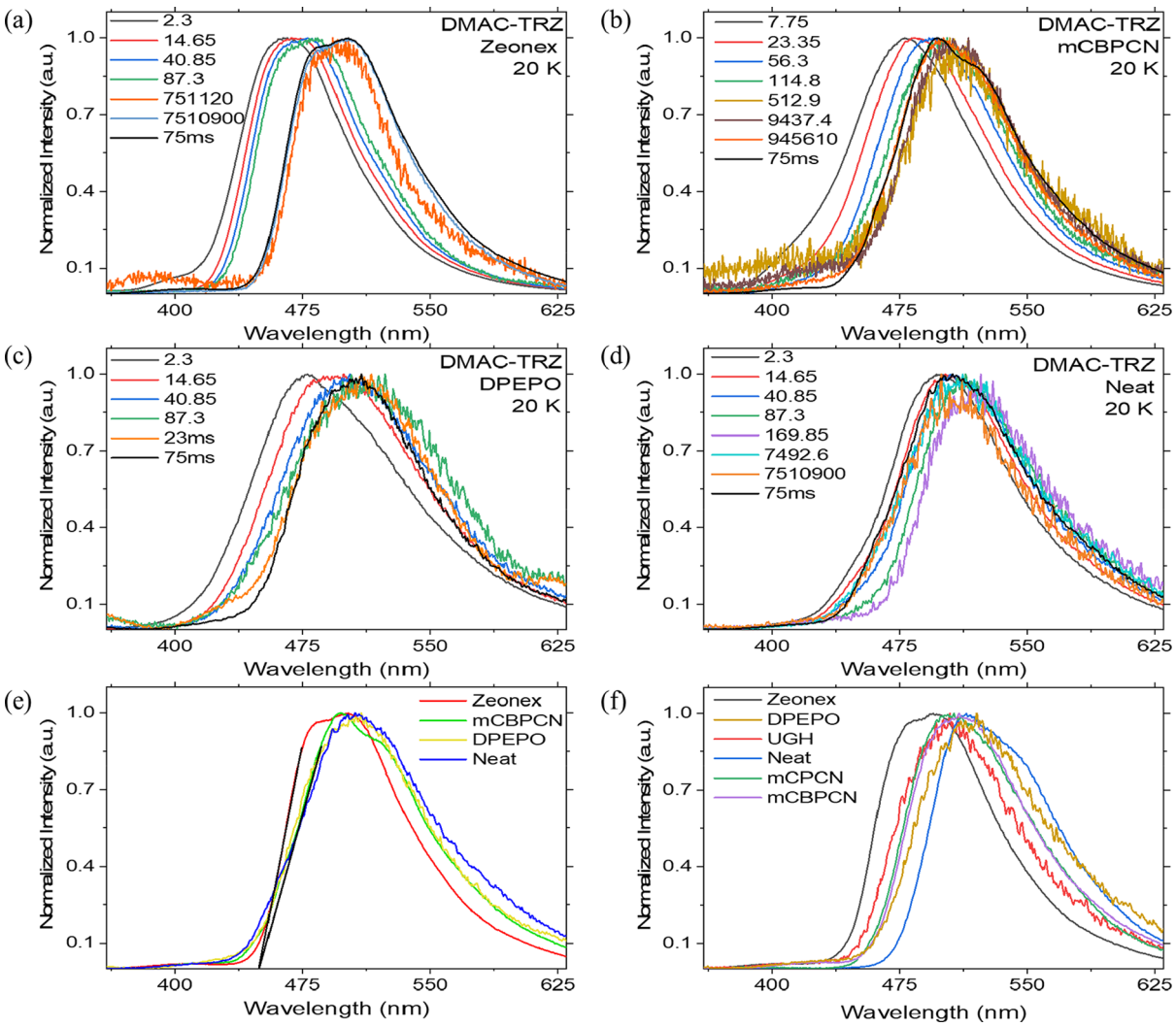

Figure 3. Time-resolved PL spectra, at 20 K (LT), of 1% w/w DMAC−TRZ in (a) Zeonex, (b) mCBPCN, and (c) DPEPO host. (d) Neat film of DMAC−TRZ. Phosphorescence spectra of DMAC−TRZ in different hosts at (e) 20 and (f) 80 K, taken at 75 ms time delay. Times given on each plot are in nanoseconds, unless stated.

fluorescence decay was fitted by two exponential terms determining the decay lifetime at 27 ns and 5.50 μs for prompt and delayed emissions, respectively. Using kinetic modeling, according to Haase *et al.*,[43] a radiative decay rate [k_F = (1.50 ± 0.08) × 10^7 s^{-1}], intersystem crossing rate [k_{ISC} = (2.50 ± 0.08) × 10^7 s^{-1}], and rISC rate [k_{rISC} = (5.1 ± 0.2) × 10^5 s^{-1}] were calculated. Emission spectra at different delayed times from these two regimes are also given (Figure S2b). The same Gaussian band shape emission spectrum is observed throughout from a single CT state, with an energy onset at 2.73 eV. In Figure S2c, we give a three-axis representation showing the energy onset and full width at half-maximum (fwhm) of the emission spectrum over time, giving an indication of the evolution over time of the DMAC−TRZ CT state distributions/contribution. The third trace, fwhm over energy onset, acts as a homogeneity indicator ("fingerprint") of the studied system. In this case, DMAC−TRZ in toluene, the data points low scatter forming the "green dot", meaning that all molecules in the system have almost the same conformation and as a result similar CT state emission energy as expected in solution.

Moving from solution to solid-state samples, various hosts were used to investigate emitter−host interactions. Five commercially available hosts that satisfy the requirement of having their singlet (S_1) and triplet (T_1) energies higher than the S_1 and T_1 energies of the emitter (Figure 1) were chosen. Thus, singlet and triplet energy transfer from the host to the guest can be achieved, *via* Förster resonance and Dexter energy transfer, while preventing quenching of delayed fluorescence (DF) by the host.

Initial samples were fabricated by a solution-processed method.[44−46] A further goal of this work is to identify any differences in the photophysical properties of DMAC−TRZ between these films and evaporated ones. In order to compare emissive behavior in solution and solid films, a neutral polymer, Zeonex, was used as a host matrix with a large free volume comparable to the MCH solution. Small-molecule rigid hosts, UGH with considerably low dielectric/polarizability, mCBPCN, mCPCN, and DPEPO with increasing dielectric/polarizability, have a larger impact on emitter's behavior (Figure 1a).

Based on the absorption spectrum (Figure S3), the CT band of the emitter is clearly observed in the Zeonex matrix, ranging between 350 and 450 nm. In neat DMAC−TRZ films, the spectrum is similar, but the onset red shifts are presumed to be due to the enhanced intermolecular interactions. In all other

https://dx.doi.org/10.1021/acsaelm.0c00514
ACS Appl. Electron. Mater. XXXX, XXX, XXX−XXX

hosts, the ground-state band has a similar shape; however, because of decreased concentration of emitters, these low-energy bands have lower intensity compared to neat films. In steady-state PL spectra, the effect of each host is more apparent. In Zeonex, the spectrum is energetically similar to that observed in nonpolar MCH solvents, onset at 427 nm, while as the host polarizability increases, the CT emission is observed at lower energy, with DPEPO having a maximum at 507 nm along with a highly broadened spectral band shape. In order to understand how the TADF mechanism is affected by each host matrix, time-resolved PL measurements were measured. The main difference between the solid state and solutions is that the DMAC−TRZ molecules (as well as the solvent) have the freedom to reorganize and reach an equilibrium dihedral angle between the donor and acceptor units according to the polarity and reorganization of the surrounding solvent molecules, while in the solid state, the rigid host matrix which cannot move locks in the emitter−neighboring the host molecule structure as a film forms. As a result, instead of having a single "equilibrium" ^{1}CT state energy (Figure S2b,c), there is a distribution of different CT states depending on emitter conformation and D−A dihedral angle, dictated by host packing and guest−host interactions, including polarizability effects. We always observe an apparent time-dependent spectral red shift of the emission band (over the first 50 ns or so, orders of magnitude slower than typical solution-state solvatochromic shifts) during the prompt decay period as well as on the early delayed emission. At later delay times, a blue shift of emission can also be seen in most cases (Figures 2 and S4). This distinct molecular behavior, in every host, can also be clearly observed by the homogeneity "fingerprint" in Figure S4 (fwhm *vs* onset). The smaller the distribution of the points, the more homogeneous the system is. Neat films have the most homogeneous environment overall. DMAC−TRZ in the Zeonex host has the highest homogeneity of prompt CT state distribution, while in mCPCN and mCBPCN, hosts give the most stable DF emission. Recent works by Dias *et al.* and Penfold *et al.* have shown that the prompt CT emission of TADF molecules undergoes an apparent dynamic red shift over the first few hundred nanoseconds arising from the heterogeneity of dihedral angles, leading to a dispersion in CT energy.[1,2] The most planar D−A molecules (reduced dihedral angle) have the more LE character and strongest excited-state coupling to the ground state, so emit to the blue at an energy close to the local donor (or acceptor) state with a faster radiative rate. However, the most orthogonal D−A molecules have the strongest CT character and therefore emit to the red at lower energy with a slower radiative rate (weak ground-state coupling). In the delayed region, the opposite is observed if the rISC-mediating local triplet state is lower in energy that the ^{3}CT. The most orthogonal D−A have the highest rISC rate, as a result they decay faster, while the planar are slower and are assigned to the late time blue shift of the emission. Introducing rigidity as a parameter, the less rigid (higher free space) the host, that is, Zeonex, the smaller the distribution of CT state energies, and so the smaller the apparent red shift in time. Dispersion is found to increase with increasing host rigidity, as shown in Figure 2.

The same behavior appears in low-temperature measurements at 80 K (Figure S5). Rigid hosts have similar CT distributions as observed in room-temperature measurements, whereas in Zeonex, the dispersion increases greatly, similar to a rigid host at room temperature (Figure S6a). Here, low temperature prevents the Zeonex chain motion, thus freezing conformational heterogeneity in DMAC−TRZ. We point out that even at low temperatures, phosphorescence emission only becomes the dominant decay mechanism in 10 ms and is not responsible for this μs blue shift.

Usually, 80 K time-resolved PL measurements are used to define the phosphorescence energy of various systems. Phosphorescence defines the lowest lying triplet state of any system, typically the triplet state of the donor, and thus, it should be the same/very similar regardless of the host. On the contrary, we observe phosphorescence to be different in every host (Figure 3f). At low temperatures, both nonradiative processes are suppressed, and delayed emission is minimized or quenched as there is less thermal energy to activate the TADF mechanism. However, in DMAC−TRZ, the lowest triplet state energy is so close to the ^{1}CT energy that there is enough thermal energy in the system, even at 80 K, to activate rISC. Thus, DF is observed even at 80 K. Also, at low temperature because of the dispersive rISC rates, DF is observed even at ms times. Consequently, the observed phosphorescence is not simple triplet state emission but a combination of both DF and phosphorescence emission, and errors are introduced into the estimate of the lowest triplet state energy of the system.

Further measurement at 20 K demonstrates that the actual lowest triplet energy of DMAC−TRZ is 2.75 eV (Figure 3e) and is host independent. Time-resolved PL spectra analysis at 20 K reveals spectral shifts mainly confined within the prompt time region, confirming this to be a combined effect of inhomogeneity and local contribution (donor emission) in the early times, as shown in Figure S7 (onset *vs* time). Based on the magnitude of the singlet triplet energy gap (ΔE_{ST}), there is a minor delayed CT contribution for a couple of 100 ns only (Figure 3).

Another indication that we are observing the actual triplet energy is the vibronic structure observed on the emission in Zeonex and mCBPCN, which indicates that the emission comes from a local excited triplet state. By comparing the two, Zeonex has only a prompt emission and phosphorescence at ms because of the highest ΔE_{ST}. mCBPCN on the other hand has a small but observable delayed contribution for some μs (even at 20 K) as the gap in this case is much lower. Nevertheless, the phosphorescence emission onset energy stabilizes at close to 1 ms, while at 80 K, the sample still shows a constant spectral shift even close to 100 ms. Similar behavior with the latter is observed in DPEPO; although the phosphorescence spectrum is not structured, the onset maintains the same value. On the contrary, neat DMAC−TRZ films have constant delayed emission, similar to the 80 K measurement, but different triplet energy onsets over longer delays. Thus, at 20 K, the temperature is low enough to minimize the rISC and prevent emission overlap between DF and phosphorescence over longer delays with the exception of neat films which must have other mechanisms contributing to the delayed part, for example, dimer formation or triplet triplet annihilation (TTA).

The above discussion clarifies the apparent host dependency of the triplet energy, but the consistent spectral shift issue adds an extra dimension to the problem. In low dielectric/polarizability hosts, the singlet triplet gap is high; as a result, the lowest lying singlet CT state is well above the local triplet. Higher dielectric/polarizability hosts not only minimize the

https://dx.doi.org/10.1021/acsaelm.0c00514
ACS Appl. Electron. Mater. XXXX, XXX, XXX−XXX

singlet triplet gap but can also cause the lowest lying CT states to fall below the lowest local triplet state, as observed weakly in the cases of mCPCN/mCBPCN but more pronounced in DPEPO/neat films (Figures 2 and S4). At 80 K, the distribution of CT states is larger than that at room temperature, during the entire time region of analyses, as can be seen in Figures S5 and S6 by an increased distribution of onsets over time. In the delayed regime (t > 100 ns), the lower temperature reduces k_{rISC} favoring rISC from the population of CT states closer to LE once there is a little excess thermal energy in the system, Figure 4. This effect was evidenced by the smaller fwhm values in the 80 K measurements compared to room temperature.

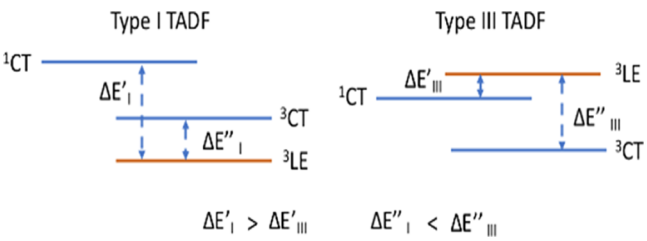

Figure 4. Schematic energy level diagrams of type I TADF (left side) and type III TADF (right side). Type II TADF, not represented here, has all the three energy levels effectively in resonance ($\Delta E' = \Delta E'' = 0$).

From the temperature-dependent decay kinetics, Figure 5, we see a clear exponential dependence in DF intensity with the magnitude of ΔE_{ST}.[47] In Zeonex, where the gap is 170 meV (Table 1), the delayed contribution is minimized at 80 K (observed by the huge drop of the delayed regime at t > 100 ns), while at 20 K, it is completely quenched and only phosphorescence is observed at longer delays. In the case of mCPCN and mCBPCN, with ΔE_{ST} at 12 and 24 meV, respectively, the drop is much lower at 80 K, compared to Zeonex, and is proportional to the gap. In 20 K, both have similar behavior and the delayed contribution is negligible. However, if there is a sizable population of CT states having a negative gap, as in DPEPO, then the drop becomes even smaller at both 80 and 20 K, not following an exponential dependence on the ST gap, but the delayed contribution to the overall emission minimizes as the temperature decreases. This is type III rISC (Figure 4) where ^{1}CT and ^{3}CT are energetically below the coupling ^{3}LE state.[17] Given that ^{3}CT must always be lower in energy than ^{1}CT, then for type III rISC, the ^{3}LE−^{3}CT gap is bigger than the ^{3}LE−^{1}CT gap and so the nonadiabatic coupling (between ^{3}CT and ^{3}LE) will become less efficient, but conversely, the ^{3}LE−^{1}CT gap is smaller than that for type I systems (CT states above ^{3}LE).[17] In the case where $|\Delta E_{ST}|$ < 50 meV, then this can be a large effective change because k_{rISC} depends exponentially on the ^{3}LE−^{1}CT gap and quadratically on the ^{3}LE−^{3}CT gap,[21] so at lower temperatures type III systems can display TADF, whereas for type I, it is quenched as the ^{3}LE−^{1}CT gap dominates (Figure 4). This is another reason why the type III states decay more slowly, but as Gibson and Penfold have calculated,[48] even at absolute zero there is still nonadiabatic coupling overcoming large ^{3}LE−^{3}CT gaps. Thus, for DPEPO, the DF temperature dependency departs from the expected exponential because the type III rISC has an important contribution to the overall DF of this system.

At this point, it is worth mentioning that another way to conclude if there is pure phosphorescence emission at longer delays is by observing the slope of the decay in this region. As seen in all cases, the slope after 1 ms gets closer to zero at 20 K, while in 80 K, the slope is still negative (Figures S6 and S7). The only film that does not follow this trend is neat because of possible contribution from dimers or TTA. The decay in both temperatures is similar, but at 20 K, it tends to reach a plateau at later times. In Figure 5, the room-temperature PL decays show how the lifetimes of the prompt and delayed emissions depend on the host and its characteristics. As expected, the prompt lifetime is similar in all cases, close to 20 ns and independent of the host. For the delayed emission, neat films have a behavior similar to DMAC−TRZ in toluene (Figure S2), again showing the low inhomogeneity of neat films (Figure S4). In DPEPO where the CT lies below the lowest triplet state, a minor decrease in the intensity of the delayed component is observed (Table 1). mCPCN and mCBPCN with minimal ΔE_{ST} are very similar, whereas Zeonex and UGH with large ΔE_{ST} results in longer delayed lifetimes as well as lower delayed contribution relative to the prompt. Further, in rigid hosts with dispersive CT energy, the DF lifetime becomes biexponential relative to DMAC−TRZ in solution and Zeonex films. DF lifetimes decrease with increasing polarizability of the rigid host, with an additional fast DF lifetime contribution having largest contribution to the total DF, while the slower DF lifetime component has a smaller contribution (Table 1).

Another phenomenon appears in all guest−host films, related to the long-time tail of the decay. By introducing a host, the long-time decay has increased lifetime (longer tail lifetime) compared to solution and neat films. Using a diluted emitter in toluene as a reference (Figure S2a), which has no tail, and comparing with the neat film which has a relatively stable and the smallest fwhm value of any solid and toluene solution (Figure S4), thus as we have seen consistently, the neat film has the smallest degree of inhomogeneous broadening and in this case, the tail phenomenon is minor and similar to toluene solution. In both cases, there is only one molecular conformation contributing to the DF regime. In neat films, we assume this to arise effectively through the "aggregated" form of solid DMAC−TRZ, giving a homogeneous environment. The main extra parameters guest−host films introduced are reduced freedom for the guest molecular rearrangement and intermolecular interactions because of smaller average distances between the DMAC−TRZ molecules, polarizability, and structural rigidity of the host. In guest−host systems, the slope of the tail tends to decrease with increasing polarizability but not proportionally (Figure S8a). As stated before in all these systems, there is a distribution of CT states based on the variety of molecular conformations, that is, dihedral angles, leading to a broad distribution of rISC rates within the films. This distribution is obviously controlled by the host environment.

In our measurements, for Zeonex, the tail slope value is shallow (more inhomogeneous), whereas for higher polarizability hosts, the slope becomes steeper and is steepest for neat films (most homogeneous). The high dielectric host (DPEPO) has only a slightly larger slope than mCPCN. To understand this, we propose a simple model based on a distribution of dihedral angle values, that is, a variety of molecular conformations (local environments) in each system giving a distribution of ΔE_{ST} and thus, rISC rates and DF lifetime values (Figure S9). In the case of mCBPCN having a

https://dx.doi.org/10.1021/acsaelm.0c00514
ACS Appl. Electron. Mater. XXXX, XXX, XXX−XXX

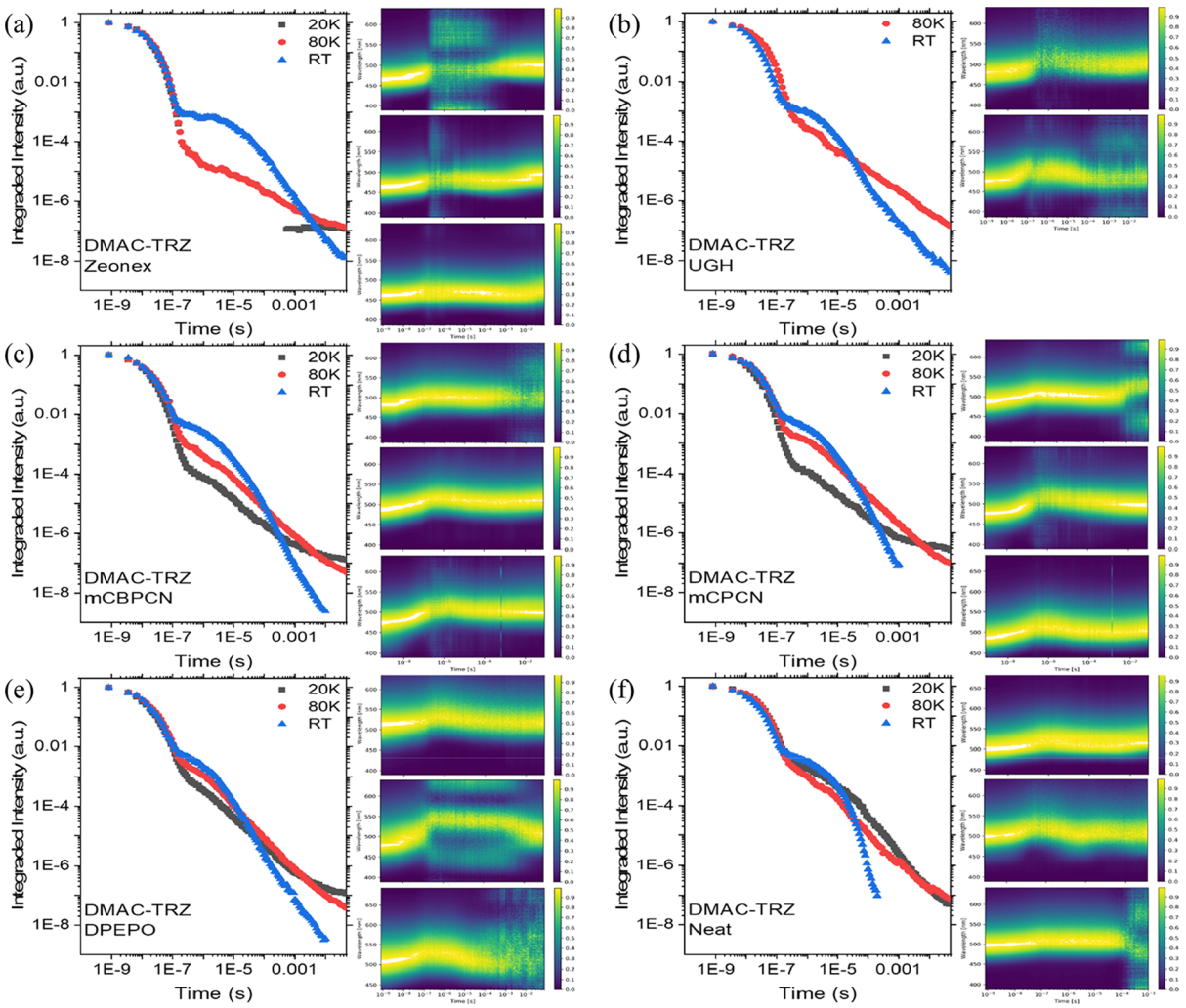

Figure 5. Time-resolved PL decays of 1% w/w DMAC−TRZ in (a) Zeonex, (b) UGH, (c) mCBPCN, (d) mCPCN, and (e) DPEPO host. (f) Neat films of DMAC−TRZ, at room temperature (cyan), 80 K (red), and 20 K (gray). On the right side of each graph, the contour plots of PL are indicated over time at 298, 80, and 20 K from top to bottom. Data points not plotted indicate signals measured, that is, below the noise floor of the iCCD detector, there is no real measurable signal at these times.

Table 1. Kinetic Modeling Results, Time Constants, and Decay Rates for Solution-Processed DMAC−TRZ Films in Different Hosts

DMAC−TRZ 1% w/w in host		Zeonex	UGH	mCBPCN	mCPCN	DPEPO	neat film	toluene[b]
spectral shift (nm)[a]	RT	8	12	17	18	19	9	0
	LT	21	26	28	24	21	14	
ΔE_{ST} (meV)[a]		170	95	24	12	−42	−42	−20
$\Delta E[T_H - T_G]$ (eV)[c]		>0.50	0.75	0.10	0.14	0.35		
τ_{prompt} (ns)		18.5	15.7	15.8	18.4	15.7	18.5	27.4
$A_{delayed}$ (%)	A_1	100	71.4	70.4	66.6	72.3	61.9	100
	A_2		28.6	29.6	33.4	27.7	38.1	
$\tau_{delayed}$ (μs)	τ_1	6.27	1.59	0.86	0.61	0.6	0.69	5.51
	τ_2		9.19	5.62	4.42	3.56	5.71	
k_F		3.3×10^7	3.8×10^7	3.0×10^7	2.6×10^7	2.9×10^7	2.5×10^7	1.5×10^7
k_{ISC}		2.1×10^7	1.3×10^7	2.0×10^7	1.8×10^7	1.8×10^7	1.8×10^7	2.5×10^7
k_{rISC}		1.7×10^5	4.8×10^5	9.3×10^5	9.6×10^5	1.1×10^6	8.1×10^5	5.1×10^5

[a]Data were extracted experimentally from the time-resolved spectra at room temperature (RT) and 80 K (LT). Spectral shift was measured by the onsets of first frame (2.3 ns) and energetically lowest lying CT frame. ΔE_{ST} was measured using the onset of the stabilized CT emission at room temperature and the onset of phosphorescence emission at 20 K. [b]DMAC−TRZ in toluene solution for comparison, concentration 20 μM. [c]$T_{H,G}$: triplet energy of host (H) and guest (G) measured at 80 and 20 K, respectively, at 80 ms time delay. UGH and Zeonex triplet energy were taken from the literature.

https://dx.doi.org/10.1021/acsaelm.0c00514
ACS Appl. Electron. Mater. XXXX, XXX, XXX−XXX

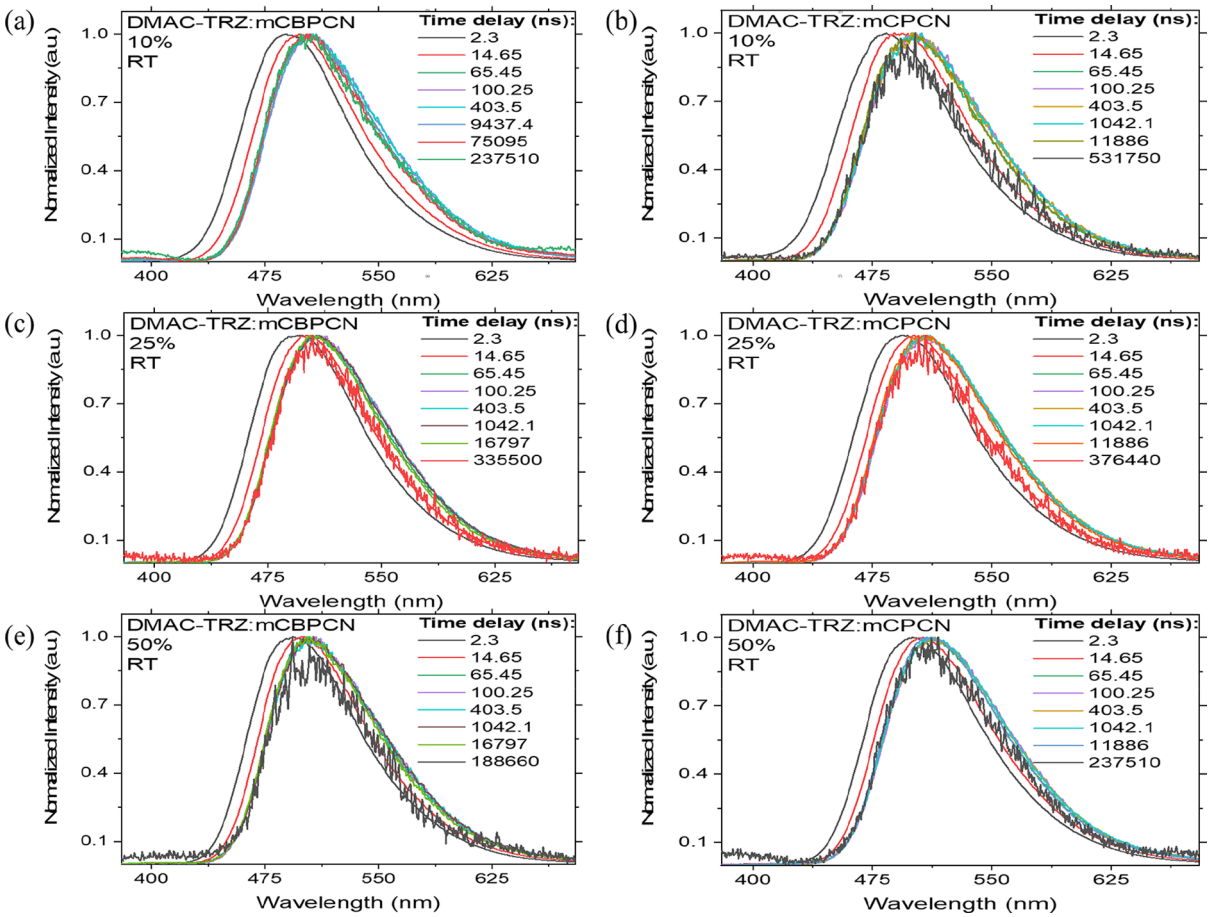

Figure 6. Time-resolved normalized PL spectra, at 298 K (RT), of DMAC−TRZ at (a) 10, (b) 25, and (c) 50% concentration in mCBPCN and at (d) 10, (e) 25, and (f) 50% concentration in mCPCN. The curves were obtained with 355 nm excitation. Times given on each plot are in nanoseconds, unless stated.

small ΔE_{ST} and faster rISC rate throughout the DF regime, the tail decays quickly, Figure S9a. We fit the tail with an arbitrary set of DF decay times (θ_1−θ_8) representing the distribution of dihedral angles. We do the same for Zeonex, Figure S9b. In this case, ΔE_{ST} is much higher and all k_{rISC} values are much smaller. Assuming that the distribution of angles is roughly the same in both hosts so that the change in ΔE_{ST} is similar, we see that if we start from a large ΔE_{ST}, increasing ΔE_{ST} has a much greater effect on ΔE_{ST} distribution than starting from a small ΔE_{ST}. If the inhomogeneity is small, similarly it will have a small effect on the distribution of ΔE_{ST}. Thus for Zeonex, each DF decay component (θ_1−θ_8) is much longer than that for mCBPCN. As shown in Figure S9d, the model approach is in good agreement with the experimental results (Figure S8a). In DPEPO, with type III TADF, the fastest k_{rISC} does not come from the lowest energy CT state which is below the ^{3}LE. As a result, the effect of disorder is more complex on the distribution of decay times.

A way to confirm that no other processes contribute to the delayed component of the time-resolved PL is laser fluence measurement. These measurements were performed over a time range of 0.5−10 μs; in this regime, the fast DF component is considered to be dominant. In all five hosts, the gradient of the power dependence measurements was close to one. Only neat films have a gradient of 1.3, at low excitation doses, which indicates the coexistence of TADF and another long-lived mechanism, such as TTA[49] (Figure S8).

From kinetic modeling, the fluorescence decay rate and k_{ISC} are similar in all cases (Table 1).[43] k_{rISC} is purely dependent on the host and how it affects the ΔE_{ST}; the higher the gap, the slower the rate is. Starting from Zeonex with a rate of $(1.7 \pm 0.1) \times 10^5$ s^{-1}, the rate increases proportionally to the gap, while DPEPO with negative ΔE_{ST} is 1 order of magnitude higher than Zeonex. According to Gibson and Penfold,[48] by casting a semiclassical (Marcus-like) approach on the second-order perturbation theory, k_{rISC} is dependent of the non-adiabatic coupling, second-order coupling connecting ^{3}LE and ^{1}CT *via* ^{3}CT and $\exp(\Delta E_{ST})^2$. Applying the calculated rates and ΔE_{ST} in our results, an excellent fit with the theory was found, Figure S10. DPEPO is the only host that does not follow the trend because of its negative gap. In this type III case, the second-order coupling is affected as the ^{1}CT state is closer to the ^{3}LE state than the ^{3}CT state, leading to $\Delta E_{TT} > \Delta E_{ST}$ (where T−T corresponds to ^{3}LE−^{3}CT), but the more temperature-sensitive process of the rISC step, controlled by the ^{1}CT−^{3}LE gap, is smaller in this case (Figure 4).

To investigate if the sample preparation method affects rISC, guest−host films of 100 nm thickness were fabricated by thermal vapor deposition and compared with solution-processed films. As hosts, mCBPCN and mCPCN were chosen because of the desirably small ΔE_{ST}, and various concentrations of the emitter in the host were studied.

Initially, steady-state measurements were performed on these films, as shown in Figure S11. PL excitation spectra

https://dx.doi.org/10.1021/acsaelm.0c00514
ACS Appl. Electron. Mater. XXXX, XXX, XXX−XXX

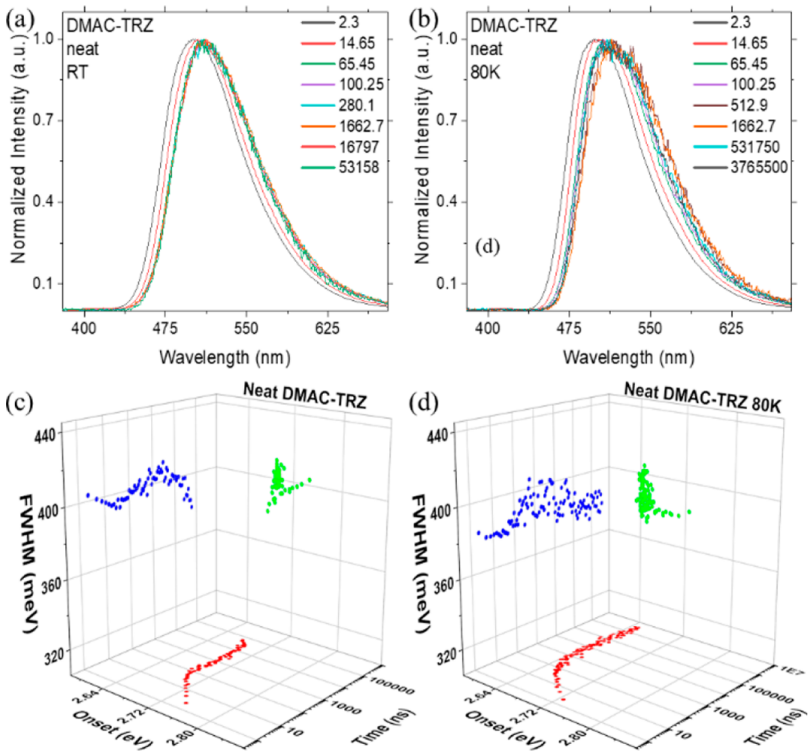

Figure 7. Time-resolved normalized PL spectra of the DMAC−TRZ neat film at (a) room temperature and (b) 80 K. Time-resolved onset energy and fwhm at (c) room temperature and (d) 80 K. The curves were obtained with 355 nm excitation. Times given on each plot are in nanoseconds, unless stated.

(dashed line) show in both hosts a band increase around 400 nm, with increasing concentration. This effect is related to the increasing amount of DMAC−TRZ in the blend, while the band is also observed in the DMAC−TRZ neat film. A slight red shift in emission spectra toward the energy of the neat DMAC−TRZ film emission at high concentrations indicates the existence of stronger intermolecular interactions with increased concentration. As in solution, the mCPCN emission spectra are slightly red-shifted compared to that of mCBPCN. Intermolecular interactions, such as dimer/aggregate formation in DMAC−TRZ neat films, can result in higher wavelength emission compared to the host−guest blends.

Figure 6 shows the time-resolved emission spectra of the host−guest evaporated films at different guest concentrations. Similar to solution-processed films, all show a prompt emission of the CT character with higher energy CT states decaying faster, giving rise to an apparent red shift in time and stabilization of the emission energy at around 100 ns. Further, smaller shifts were observed, which are attributed to states at the edges of the D−A dihedral angle distribution. These shifts are only around 2 and 3 nm, indicating a far smaller distribution compared to solution-processed films. For DMAC−TRZ:mCBPCN films (after stabilization >100 ns), the onset of CT emission is found to be the same at all concentrations, around 455 nm. However, in mCPCN blends, the onset energy of stabilized CT emission decreases with increasing concentration (Figure 8), which suggests that because of different packings of the two hosts, the intermolecular interactions are limited in the mCBPCN matrix, while mCPCN leads to more aggregation even in low concentrations. On the contrary, at 80 K, both guest−host systems have similar behavior (Figures S12 and S13), which may indicate an activated triplet hopping to dimer/aggregate sites.

In neat films, the intermolecular interactions are considered the prevailing state. In Figure 7a,c, the time-resolved emission spectra of DMAC−TRZ at room temperature reveal a red shift of prompt CT during the first 100 ns. After that, a stable CT state is observed until 100 μs with the onset at 461 nm, close to that observed in the 50% DMAC−TRZ:mCPCN blend. Thus, by increasing the concentration in mCPCN blends, we approach the behavior of DMAC−TRZ neat films. At 80 K, spectral shift trends are very similar to those at room temperature, with slightly larger shifts, although the emission has a longer lifetime, allowing us to see even later time emission (Figure 7b). After 100 μs, the emission spectra evolve a stable vibronic structure, which is an indication of phosphorescence emission taking over. The phosphorescence spectra of the neat film have an onset at 472 nm, similar to the solution-processed films at 80 K, but much longer than that observed at 20 K (onset 450 nm), again suggestive of thermally activated triplet migration to the low-energy dimer/aggregate sites.

Time-resolved decays at room and low temperature for the emitter in mCPCN are shown in Figure S14. At 10% concentration, the reduction of the delayed contribution at 80 K compared to room temperature is significant. As concentration increases, the DF decreases and becomes comparable to neat film levels. This is related to the stronger intermolecular interaction; at higher concentrations leading to increased excited-state quenching, both prompt and delayed lifetimes shorten. Different behavior is observed in DMAC−TRZ:mCBPCN films (Figure S15). At 10% concentration, the drop in the delayed contribution is comparable to that seen in the 1% solution-processed film, while increasing the concen-

https://dx.doi.org/10.1021/acsaelm.0c00514
ACS Appl. Electron. Mater. XXXX, XXX, XXX−XXX

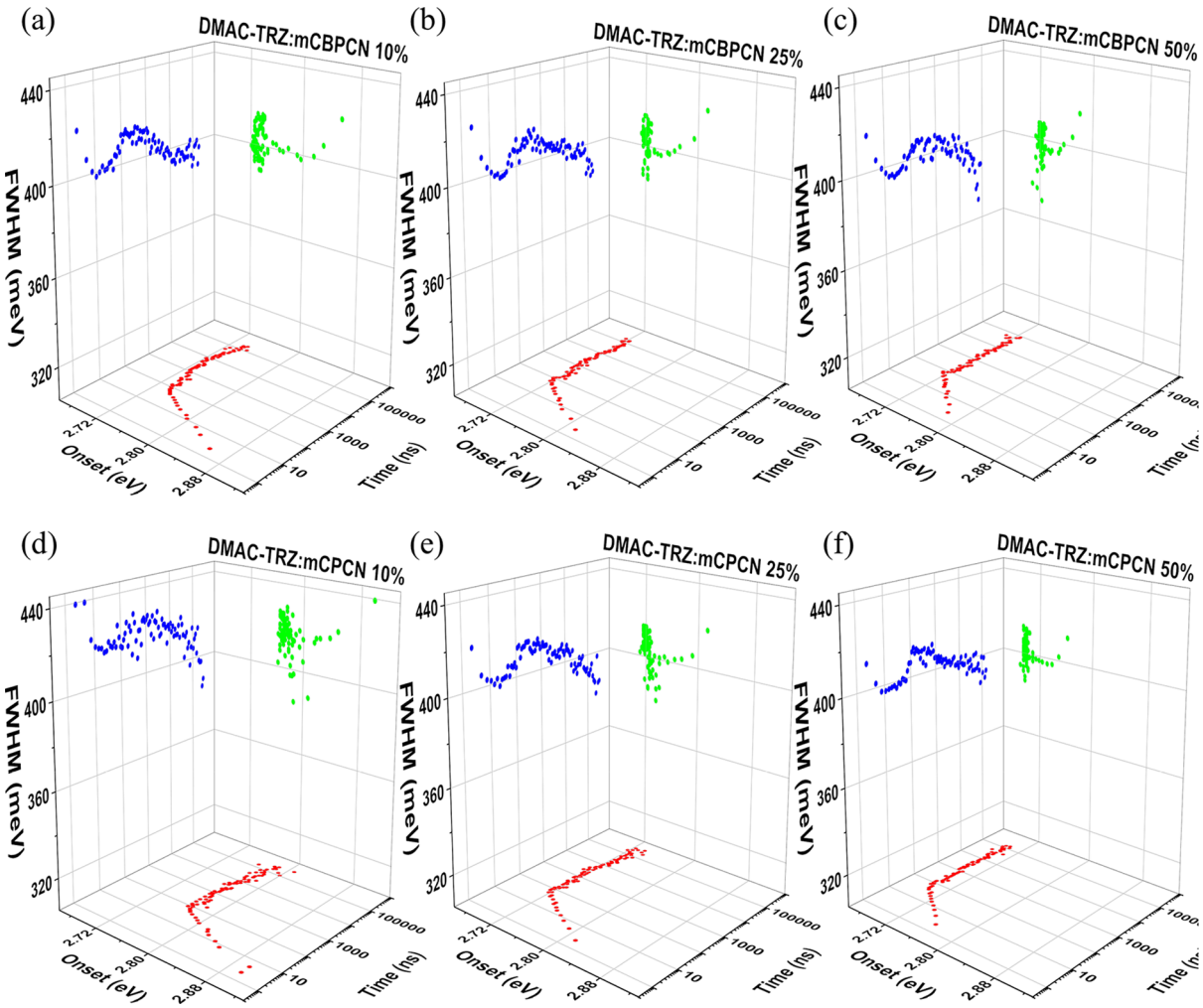

Figure 8. Time-resolved onset energy and fwhm of (a) 10, (b) 25, and (c) 50% evaporated DMAC−TRZ in mCBPCN and (d) 10, (e) 25, and (f) 50% evaporated DMAC−TRZ in the mCPCN host.

tration of the emitter yields a negligible change. This unique behavior points to the peculiarity of mCBPCN as a host. Based on our finding so far, increasing the concentration of DMAC−TRZ in any host leads to aggregation/excimer formation, which changes the system behavior and induces excited-state quenching. On the other hand, in mCBPCN, this effect is minimized, which implies the existence of an optimized packing between DMAC−TRZ and mCBPCN even at higher concentrations. This is seen as a stable fwhm and delayed emission onset energy even at long times, indicating a singular emitting species (Figure 8).

The packing effect can be further explored by comparing room- and low-temperature decays in the two different systems using neat films as a reference system (Figure 9). In mCPCN, the prompt lifetime decreases with increasing DMAC−TRZ concentration, an indication of increasing quenching, whereas in mCBPCN, it remains constant at room temperature. The delayed emission in mCPCN has a similar trend, decreasing the time onset with increased concentration, that is, less DF indicative of prompt excited-state quenching, whereas in mCBPCN, the delayed emission onset increases with increased concentration, indicating a higher delayed emission contribution because of an increased number of excitations in the system. Comparing low-temperature time-resolved decays, both systems show increased delayed emission contribution with increased concentration, and at 50% emitter concentration, the response is indistinguishable compared to neat films.

The results of kinetic modeling of these data are shown in Table 2. The prompt lifetime of mCBPCN is constant, while in mCPCN, it decreases with increasing concentration. In the delayed regime, the amplitude of both components increases with increasing concentration for mCBPCN, whereas the opposite occurs in the case of mCPCN. On the contrary, the lifetimes for mCBPCN decrease with increasing concentration, whereas in mCPCN, they remain constant. This we take to imply that the quenching of prompt states in mCPCN is controlled by excited-state migration to quenching sites.

The PLQY of all samples is given in Table 2. The integrating sphere measurement is sensitive to sample absorption; for this reason, two different excitation wavelengths were used: 370 nm where the absorbance is high enough at all concentrations and 400 nm which excites the direct CT transition but has limited absorbance at low concentration. In the case of mCBPCN with increased concentration, a minor decrease in PLQY is observed with 370 nm excitation. By directly exciting the CT band, at 400 nm, the optimum PLQY is found, whereas at 370 nm, absorption from the host causes some extrinsic losses. Subsequently, PLQY values close to unity at the 25% concentration film are found, while at 50%, it is only slightly

https://dx.doi.org/10.1021/acsaelm.0c00514
ACS Appl. Electron. Mater. XXXX, XXX, XXX−XXX

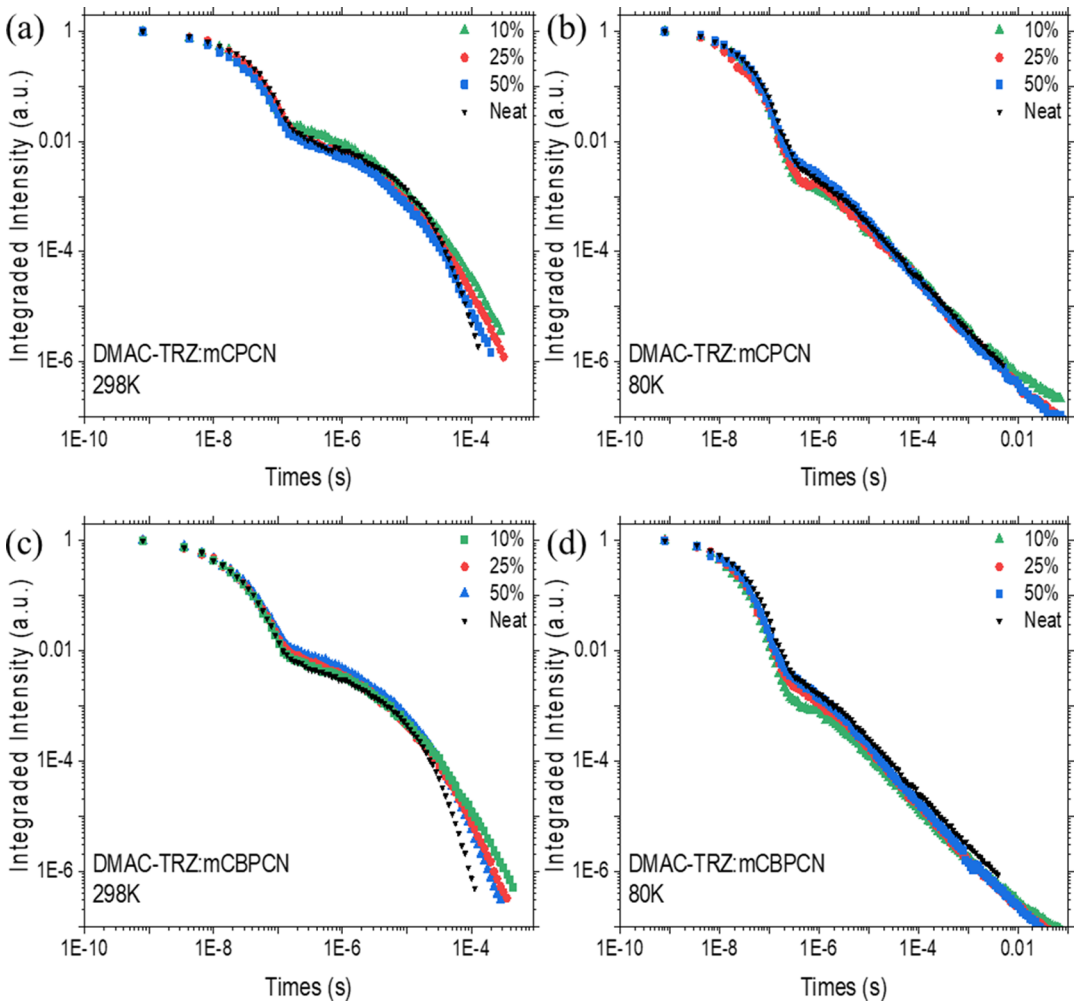

Figure 9. Time-resolved PL decays of various concentrations of DMAC−TRZ in mCPCN at (a) 298 and (b) 80 K and mCBPCN at (c) 298 and (d) 80 K.

Table 2. Kinetic Modeling Results, Time Constants, and Decay Rates for Various Concentrations of Evaporated DMAC−TRZ Films Diluted in mCBPCN, mCPCN Hosts, and Neat Film

host		mCBPCN			mCPCN			none
DMAC−TRZ conc. (%)		10	25	50	10	25	50	100
spectral shift (nm)[a]	RT	20	17	13	20	17	13	12
	LT	24	24	27	25	24	25	14
ΔE_{ST} (meV)[a]		−42	−42	−42	12	−42	−60	−60
PLQY (%)[b]	370	87	85	83				
	400		98	87		90	80	75
τ_{prompt} (ns)		19	18	18	25	23	19	29
$A_{delayed}$ (%)	A_1	75	77	75	79	80	81	69
	A_2	25	23	25	21	20	19	31
$\tau_{delayed}$ (μs)	τ_1	1.5	1.2	1.1	1.2	1.3	1.3	1.6
	τ_2	9.5	8.2	8.0	8.6	8.3	8.2	9.2
k_F (s^{-1})		2.2×10^7	2.1×10^7	1.8×10^7	1.2×10^7	1.7×10^7	1.8×10^7	1.2×10^7
k_{ISC} (s^{-1})		2.1×10^7	2.0×10^7	2.1×10^7	2.2×10^7	2.0×10^7	2.4×10^7	1.8×10^7
k_{rISC} (s^{-1})		7.3×10^5	8.3×10^5	9.0×10^5	9.0×10^5	8.8×10^5	8.6×10^5	5.8×10^5

[a]Data were extracted experimentally from the time-resolved spectra at room temperature (RT) and 80 K (LT). Spectral shift was measured by the onsets of first frame (2.3 ns) and energetically lowest lying CT frame. ΔE_{ST} was measured using the onset of the stabilized CT emission at room temperature and the onset of phosphorescence emission at 20 K. [b]PLQY of films was measured in an intergraded sphere connected with Fluorolog-3 under two excitations, 370 and 400 nm.

below 0.9. At 10% concentration, the absorption is limited and the value is unreliable, but following the trend seen with 370 nm excitation the value should be similar to 25%, *ca.* unity. In mCPCN, to measure the maximum PLQY values, only the

https://dx.doi.org/10.1021/acsaelm.0c00514
ACS Appl. Electron. Mater. XXXX, XXX, XXX−XXX

direct CT excitation PLQYs, at 400 nm, were obtained. Compared to mCBPCN, there is a reduction by around 10−15% at all concentrations because of possible dimer/excimer excitation. For comparison, in neat films, the PLQY is found to be only 0.75.

PLQY values combined with calculated ΔE_{ST} and kinetic rISC rates reveal the possible performance of the optimum emitter concentration in a device. In the case of mCBPCN, the ΔE_{ST} is constant, the PLQY decreases only at 50% concentration, and the fluorescence rate follows the same trend. rISC increases slightly with increased concentration, whereas intersystem crossing is stable.[43] On the other hand, mCPCN has an increasingly negative ΔE_{ST}, a higher decrease of PLQY accompanied with an increasing fluorescence rate but also increasing k_{ISC} with increased concentration. k_{rISC} is slightly decreasing and moving toward the neat film rate, while intersystem crossing is constant. Therefore, mCBPCN constantly shows higher performance, especially in higher concentrations as the optimum host for DMAC−TRZ in comparison to mCPCN and neat films. The biphenyl linking group between the carbazole units makes mCBPCN more sterically bulky and thus prevents DMAC−TRZ dimer/aggregate formation.

■ CONCLUSIONS

An in-depth photophysical analysis of DMAC−TRZ behavior in a variety of hosts, in both solution-processed and evaporated films, has been presented. The good TADF performance of the emitter is reflected in solution measurements with a high DF contribution and strong k_{rISC}. From the solvatochromic behavior of the low-energy absorption feature, we determine that they are two close lying states, one with CT character and the other a local nπ* state. The CT state undergoes red shift with increasing polarity with a rapidly diminishing oscillator strength. This indicates state mixing between these two lowest energy states, which imparts oscillator strength to the CT transition and is why in low polar environments DMAC−TRZ has high PLQY. Similar behavior was observed in the solid state with some extra parameters affecting the emitter's performance. In solution-processed films, host packing is the main factor that leads to dispersion of CT energy, ΔE_{ST}, and k_{rISC}. In the flexible Zeonex matrix, the packing effects are very weak, while in both low and high dielectric small-molecule hosts, it is dominant. In the rigid hosts, we also observed an additional delayed lifetime component, which decreases with increasing dielectric. At low temperature (80 K), the inhomogeneity is more obvious because of the reduced thermal energy required for rISC, so that states with large ΔE_{ST} have far longer delayed emission lifetimes. The presence of dimer/aggregate states is seen in most hosts, leading to prompt emission quenching and concomitant reduction in DF. However, in neat DMAC−TRZ films where intermolecular interaction must dominate, we find the smallest degree of inhomogeneity because of this. In addition, we demonstrate that in the presence of these lower energy states, phosphorescence emission can become more difficult to measure especially when ΔE_{ST} is very small, requiring very low-temperature measurements to complete quenching of all DF and prevent triplet migration to dimer/aggregates to reveal the actual lowest lying triplet of the system. In this way, we prove that the triplet energy of the emitter does not depend on the host matrix. For neat films, we also find a contribution of DF coming from TTA (Figure S8) highlighting the possible migration of triplet states in these systems, especially at high concentrations and neat films.

We give an explanation of the DF tail phenomenon, which is shown to be related to the guest−host interactions. In DMAC−TRZ solution and neat films, the phenomenon does not exist, whereas in the guest−host systems, it is always present. We find that the smaller the ΔE_{ST} is, the shorter the lifetime of the tail, showing that the ΔE_{ST} inhomogeneity introduced by packing to the D−A dihedral angle is small when ΔE_{ST} is small so that the resultant distribution in k_{rISC} is small and the tail decays quickly, whereas when ΔE_{ST} is large, the disorder-induced energetic distribution is large, leading to a wide distribution of k_{rISC} and subsequently a long slowly decaying tail. Also, concentration dependence studies verify that the smaller the concentration of the host in the system, the shorter the lifetime of the tail. We also show how the type I and type III TADF materials behave differently under the influence of host packing.

The comparison between solution-processed and evaporated films reveals the importance of the fabrication method on packing as the evaporated film CT energy distribution is minimized as seen in room-temperature time-resolved measurements. Exploring two similar hosts, mCBPCN and mCPCN in evaporated guest−host systems, a surprising inconsistent behavior appears. Because of more optimal packing, mCBPCN prevents aggregation, and thus, quenching of prompt emission and the delayed emission contributions increases with increasing concentration. On the other hand, mCPCN has indications of intermolecular interactions even in low concentrations; thus, the delayed emission contribution decreases with increasing concentration. A combination of delayed emission contribution and higher PLQY values through its novel packing mechanism makes mCBPCN an ideal host of the DMAC−TRZ system.

This study provides new insights and understanding into the guest−host effects on TADF emitters and promotes a deeper knowledge on how optimization on material design and proper combination of guest−host characteristics can improve the overall performance of a TADF molecule.

■ ASSOCIATED CONTENT

Supporting Information

The Supporting Information is available free of charge at https://pubs.acs.org/doi/10.1021/acsaelm.0c00514.

Experimental methods; normalized absorption spectra; time-resolved PL decay and spectra of 20 μM DMAC−TRZ solution in toluene; normalized absorption and fluorescence spectrum of DMAC−TRZ; time-resolved onset energy and fwhm of DMAC−TRZ; time-resolved PL spectra; time-resolved PL decays of DMAC−TRZ; theoretical approach of the CT distribution; linear relation between k_{rISC} and $(\Delta E_{ST})^2$; photoluminescence excitation spectra collected at 500 nm and photoluminescence spectra excited at 340 nm; time-resolved normalized emission spectra at 80 K of DMAC−TRZ:mCPCN; time-resolved PL decays of DMAC−TRZ in mCBPCN; and phosphorescence spectra of mCPCN and mCBPCN (PDF)

https://dx.doi.org/10.1021/acsaelm.0c00514
ACS Appl. Electron. Mater. XXXX, XXX, XXX−XXX

■ AUTHOR INFORMATION

Corresponding Author

Andrew P. Monkman − *Department of Physics, Durham University, Durham DH1 3LE, U.K.;* orcid.org/0000-0002-0784-8640; Email: a.p.monkman@durham.ac.uk

Authors

Kleitos Stavrou − *Department of Physics, Durham University, Durham DH1 3LE, U.K.;* orcid.org/0000-0001-5868-3324

Larissa G. Franca − *Department of Physics, Durham University, Durham DH1 3LE, U.K.*

Complete contact information is available at: https://pubs.acs.org/10.1021/acsaelm.0c00514

Author Contributions

K.S. and L.G.F. contributed equally. K.S. and L.G.F. performed all-thin-film fabrication, photophysical measurements, and data analysis. A.P.M. conceived the project and analyzed data. The manuscript was written through contributions of all authors. All authors have given approval to the final version of the manuscript.

Notes

The authors declare no competing financial interest.

■ ACKNOWLEDGMENTS

We thank Prof Ken-Tsung Wong for the very kind gift of materials. We would like to acknowledge the EU's Horizon 2020 for funding the TADFlife project under grant agreement no. 812872 and A.P.M. thanks the EPSRC for funding under project EP/P012167/1.

■ ABBREVIATIONS

DF, delayed fluorescence; TADF, thermally activated delayed fluorescence; PL, photoluminescence; D−A, donor−acceptor; fwhm, full width at half-maximum; k_{ISC}, intersystem crossing rate; k_{rISC}, reverse intersystem crossing rate; ΔE_{ST}, singlet−triplet energy gap; ^{1,3}CT, singlet triplet charge-transfer state; ^{1,3}LE, local excited singlet triplet state; HOMO, highest occupied molecular orbital; LUMO, lowest unoccupied molecular orbital; TTA, triplet−triplet annihilation; PLQY, photoluminescence quantum yield; DMAC, 9,9-dimethyl-9,10-dihydroacridine; TRZ, 2,4,6-triphenyl-1,3,5-triazine; MCH, methylcyclohexane; DCM, dichloromethane; DPEPO, bis[2-(diphenylphosphino)phenyl]ether oxide; UGH, *m*-bis-(triphenylsilyl)benzene; mCPCN, [9-(3-(9*H*-carbazol-9-yl)-phenyl)-9*H*carbazole-3-carbonitrile]; mCBPCN, 9-(30-(9*H*-carbazole-9-yl)-5-cyano[1,10-biphenyl]-3-yl)-9*H*-carbazole-3-carbonitrile

■ REFERENCES

(1) Northey, T.; Stacey, J.; Penfold, T. J. The Role of Solid State Solvation on the Charge Transfer State of a Thermally Activated Delayed Fluorescence Emitter. *J. Mater. Chem. C* **2017**, *5*, 11001−11009.

(2) Dias, F. B.; Santos, J.; Graves, D. R.; Data, P.; Nobuyasu, R. S.; Fox, M. A.; Batsanov, A. S.; Palmeira, T.; Berberan-Santos, M. N.; Bryce, M. R.; Monkman, A. P. The Role of Local Triplet Excited States and D-A Relative Orientation in Thermally Activated Delayed Fluorescence: Photophysics and Devices. *Adv. Sci.* **2016**, *3*, 1600080.

(3) Yang, Z.; Mao, Z.; Xie, Z.; Zhang, Y.; Liu, S.; Zhao, J.; Xu, J.; Chi, Z.; Aldred, M. P. Recent Advances in Organic Thermally Activated Delayed Fluorescence Materials. *Chem. Soc. Rev.* **2017**, *46*, 915−1016.

(4) Colella, M.; Pander, P.; Pereira, D. D. S.; Monkman, A. P. Interfacial TADF Exciplex as a Tool to Localize Excitons, Improve Efficiency, and Increase OLED Lifetime. *ACS Appl. Mater. Interfaces* **2018**, *10*, 40001−40007.

(5) Adachi, C.; Baldo, M. A.; Thompson, M. E.; Forrest, S. R. Nearly 100% Internal Phosphorescence Efficiency in an Organic Light Emitting Device. *J. Appl. Phys.* **2001**, *90*, 5048−5051.

(6) Lakowicz, J. R. *Principles of Fluorescence Spectroscopy*; Springer: US, 2007.

(7) Méhes, G.; Nomura, H.; Zhang, Q.; Nakagawa, T.; Adachi, C. Enhanced Electroluminescence Efficiency in a Spiro-Acridine Derivative through Thermally Activated Delayed Fluorescence. *Angew. Chem. Int. Ed.* **2012**, *51*, 11311−11315.

(8) Wang, H.; Xie, L.; Peng, Q.; Meng, L.; Wang, Y.; Yi, Y.; Wang, P. Novel Thermally Activated Delayed Fluorescence Materials-Thioxanthone Derivatives and Their Applications for Highly Efficient OLEDs. *Adv. Mater.* **2014**, *26*, 5198−5204.

(9) Liu, Y.; Zhan, G.; Liu, Z.-W.; Bian, Z.-Q.; Huang, C.-H. Room-Temperature Phosphorescence from Purely Organic Materials. *Chin. Chem. Lett.* **2016**, *27*, 1231−1240.

(10) Dias, F. B.; Bourdakos, K. N.; Jankus, V.; Moss, K. C.; Kamtekar, K. T.; Bhalla, V.; Santos, J.; Bryce, M. R.; Monkman, A. P. Triplet Harvesting with 100% Efficiency by Way of Thermally Activated Delayed Fluorescence in Charge Transfer OLED Emitters. *Adv. Mater.* **2013**, *25*, 3707−3714.

(11) Walden, M. T.; Pander, P.; Yufit, D. S.; Dias, F. B.; Williams, J. A. G. Homoleptic platinum(ii) complexes with pyridyltriazole ligands: excimer-forming phosphorescent emitters for solution-processed OLEDs. **2019**, *7*, 6592−6606. DOI: DOI: 10.1039/c9tc00768g.

(12) Yang, B. X.; Yao, C.; Zhou, G. Highly Efficient Phosphorescent Materials Based on Platinum Complexes and Their Application in Organic Light-Emitting Devices (OLEDs). *Platin. Met. Rev.* **2013**, *57*, 2−16.

(13) Mao, H.-T.; Li, G.-F.; Shan, G.-G.; Wang, X.-L.; Su, Z.-M. Recent Progress in Phosphorescent Ir(III) Complexes for Nondoped Organic Light-Emitting Diodes. *Coord. Chem. Rev.* **2020**, *413*, 213283.

(14) Baldo, M. A.; O'Brien, D. F.; You, Y.; Shoustikov, A.; Sibley, S.; Thompson, M. E.; Forrest, S. R. Highly Efficient Phosphorescent Emission from Organic Electroluminescent Devices. *Nature* **1998**, *395*, 151−154.

(15) Santos, P. L.; Ward, J. S.; Data, P.; Batsanov, A. S.; Bryce, M. R.; Dias, F. B.; Monkman, A. P. Engineering the Singlet-Triplet Energy Splitting in a TADF Molecule. *J. Mater. Chem. C* **2016**, *4*, 3815−3824.

(16) Dias, F. B.; Penfold, T. J.; Monkman, A. P. Photophysics of Thermally Activated Delayed Fluorescence Molecules. *Methods Appl. Fluoresc.* **2017**, *5*, 012001.

(17) Etherington, M. K.; Gibson, J.; Higginbotham, H. F.; Penfold, T. J.; Monkman, A. P. Revealing the spin-vibronic coupling mechanism of thermally activated delayed fluorescence. *Nat. Commun.* **2016**, *7*, 13680.

(18) Grabowski, Z. R.; Rotkiewicz, K.; Rettig, W. Structural Changes Accompanying Intramolecular Electron Transfer: Focus on Twisted Intramolecular Charge-Transfer States and Structures. *Chem. Rev.* **2003**, *103*, 3899−4032.

(19) Cui, L. S.; Nomura, H.; Geng, Y.; Kim, J. U.; Nakanotani, H.; Adachi, C. Controlling Singlet-Triplet Energy Splitting for Deep-Blue Thermally Activated Delayed Fluorescence Emitters. *Angewandte* **2017**, *56*, 1571−1575.

(20) Tao, Y.; Yuan, K.; Chen, T.; Xu, P.; Li, H.; Chen, R.; Zheng, C.; Zhang, L.; Huang, W. Thermally Activated Delayed Fluorescence Materials Towards the Breakthrough of Organoelectronics. *Adv. Mater.* **2014**, *26*, 7931−7958.

(21) Gibson, J.; Monkman, A. P.; Penfold, T. J. The Importance of Vibronic Coupling for Efficient Reverse Intersystem Crossing in Thermally Activated Delayed Fluorescence Molecules. *ChemPhysChem* **2016**, *17*, 2956−2961.

(22) dos Santos, P. L.; Ward, J. S.; Congrave, D. G.; Batsanov, A. S.; Eng, J.; Stacey, J. E.; Penfold, T. J.; Monkman, A. P.; Bryce, M. R. Triazatruxene: A Rigid Central Donor Unit for a D-A3 Thermally Activated Delayed Fluorescence Material Exhibiting Sub-Microsecond Reverse Intersystem Crossing and Unity Quantum Yield via Multiple Singlet-Triplet State Pairs. *Adv. Sci.* **2018**, *5*, 1700989.
(23) Yu, L.; Wu, Z.; Xie, G.; Zhong, C.; Zhu, Z.; Cong, H.; Ma, D.; Yang, C. Achieving a balance between small singlet-triplet energy splitting and high fluorescence radiative rate in a quinoxaline-based orange-red thermally activated delayed fluorescence emitter. *Chem. Commun.* **2016**, *52*, 11012−11015.
(24) Cai, X.; Gao, B.; Li, X.-L.; Cao, Y.; Su, S.-J. Singlet-Triplet Splitting Energy Management via Acceptor Substitution: Complanation Molecular Design for Deep-Blue Thermally Activated Delayed Fluorescence Emitters and Organic Light-Emitting Diodes Application. *Adv. Funct. Mater.* **2016**, *26*, 8042−8052.
(25) Lin, T. A.; Chatterjee, T.; Tsai, W. L.; Lee, W. K.; Wu, M. J.; Jiao, M.; Pan, K. C.; Yi, C. L.; Chung, C. L.; Wong, K. T.; Wu, C. C. Sky-Blue Organic Light Emitting Diode with 37% External Quantum Efficiency Using Thermally Activated Delayed Fluorescence from Spiroacridine-Triazine Hybrid. *Adv. Mater.* **2016**, *28*, 6976−6983.
(26) Kawamura, Y.; Brooks, J.; Brown, J. J.; Sasabe, H.; Adachi, C. Intermolecular Interaction and a Concentration-Quenching Mechanism of Phosphorescent Ir(III) Complexes in a Solid Film. *Phys. Rev. Lett.* **2006**, *96*, 11−14.
(27) Lakowicz, J. R. Quenching of Fluorescence. *Principles of Fluorescence Spectroscopy*; Springer, 2006; pp 277−330.
(28) Méhes, G.; Goushi, K.; Potscavage, W. J.; Adachi, C. Influence of Host Matrix on Thermally-Activated Delayed Fluorescence: Effects on Emission Lifetime, Photoluminescence Quantum Yield, and Device Performance. *Org. Electron.* **2014**, *15*, 2027−2037.
(29) Albrecht, K.; Matsuoka, K.; Fujita, K.; Yamamoto, K. Carbazole Dendrimers as Solution-Processable Thermally Activated Delayed-Fluorescence Materials. **2015**, *54*.5677 DOI: DOI: 10.1002/anie.201500203.
(30) Chaskar, A.; Chen, H.-F.; Wong, K.-T. Bipolar Host Materials: A Chemical Approach for Highly Efficient Electrophosphorescent Devices. *Adv. Mater.* **2011**, *23*, 3876−3895.
(31) Masui, K.; Nakanotani, H.; Adachi, C. Analysis of Exciton Annihilation in High-Efficiency Sky-Blue Organic Light-Emitting Diodes with Thermally Activated Delayed Fluorescence. *Org. Electron.* **2013**, *14*, 2721−2726.
(32) Jankus, V.; Chiang, C.-J.; Dias, F.; Monkman, A. P. Deep Blue Exciplex Organic Light-Emitting Diodes with Enhanced Efficiency; P-Type or E-Type Triplet Conversion to Singlet Excitons? *Adv. Mater.* **2013**, *25*, 1455−1459.
(33) Zheng, Y.; Batsanov, A. S.; Jankus, V.; Dias, F. B.; Bryce, M. R.; Monkman, A. P. Bipolar Molecules with High Triplet Energies: Synthesis, Photophysical, and Structural Properties. *J. Org. Chem.* **2011**, *76*, 8300−8310.
(34) Jankus, V.; Data, P.; Graves, D.; McGuinness, C.; Santos, J.; Bryce, M. R.; Dias, F. B.; Monkman, A. P. Highly Efficient TADF OLEDs: How the Emitter-Host Interaction Controls Both the Excited State Species and Electrical Properties of the Devices to Achieve near 100% Triplet Harvesting and High Efficiency. *Adv. Funct. Mater.* **2014**, *24*, 6178−6186.
(35) dos Santos, P. L.; Ward, J. S.; Bryce, M. R.; Monkman, A. P. Using Guest-Host Interactions To Optimize the Efficiency of TADF OLEDs. *J. Phys. Chem. Lett.* **2016**, *7*, 3341−3346.
(36) dos Santos, P. L.; Etherington, M. K.; Monkman, A. P. Chemical and Conformational Control of the Energy Gaps Involved in the Thermally Activated Delayed Fluorescence Mechanism. *J. Mater. Chem. C* **2018**, *6*, 4842−4853.
(37) Cotts, B. L.; McCarthy, D. G.; Noriega, R.; Penwell, S. B.; Delor, M.; Devore, D. D.; Mukhopadhyay, S.; De Vries, T. S.; Ginsberg, N. S. Tuning Thermally Activated Delayed Fluorescence Emitter Photophysics through Solvation in the Solid State. *ACS Energy Lett.* **2017**, *2*, 1526−1533.
(38) Tsai, W.-L.; Huang, M.-H.; Lee, W.-K.; Hsu, Y.-J.; Pan, K.-C.; Huang, Y.-H.; Ting, H.-C.; Sarma, M.; Ho, Y.-Y.; Hu, H.-C.; Chen, C.-C.; Lee, M.-T.; Wong, K.-T.; Wu, C.-C. A Versatile Thermally Activated Delayed Fluorescence Emitter for Both Highly Efficient Doped and Non-Doped Organic Light Emitting Devices. *Chem. Commun.* **2015**, *51*, 13662−13665.
(39) Woon, K.-L.; Yi, C.-L.; Pan, K.-C.; Etherington, M. K.; Wu, C.-C.; Wong, K.-T.; Monkman, A. P. Intramolecular Dimerization Quenching of Delayed Emission in Asymmetric D-D′-A TADF Emitters. *J. Phys. Chem. C* **2019**, *123*, 12400−12410.
(40) Lyskov, I.; Marian, C. M. Climbing up the Ladder: Intermediate Triplet States Promote the Reverse Intersystem Crossing in the Efficient TADF Emitter ACRSA. *J. Phys. Chem. C* **2017**, *121*, 21145−21153.
(41) De Sa Pereira, D.; Menelaou, C.; Danos, A.; Marian, C.; Monkman, A. P. Electroabsorption Spectroscopy as a Tool for Probing Charge Transfer and State Mixing in Thermally Activated Delayed Fluorescence Emitters. *J. Phys. Chem. Lett.* **2019**, *10*, 3205−3211.
(42) Ren, X.; Li, J.; Holmes, R. J.; Djurovich, P. I.; Forrest, S. R.; Thompson, M. E. Ultrahigh Energy Gap Hosts in Deep Blue Organic Electrophosphorescent Devices. *Chem. Mater.* **2004**, *16*, 4743−4747.
(43) Haase, N.; Danos, A.; Pflumm, C.; Morherr, A.; Stachelek, P.; Mekic, A.; Brütting, W.; Monkman, A. P. Kinetic Modeling of Transient Photoluminescence from Thermally Activated Delayed Fluorescence. *J. Phys. Chem. C* **2018**, *122*, 29173−29179.
(44) Colella, M.; Pander, P.; Monkman, A. P. Solution Processable Small Molecule Based TADF Exciplex OLEDs. *Org. Electron.* **2018**, *62*, 168−173.
(45) Lee, C. W.; Lee, J. Y. High Quantum Efficiency in Solution and Vacuum Processed Blue Phosphorescent Organic Light Emitting Diodes Using a Novel Benzofuropyridine-Based Bipolar Host Material. *Adv. Mater.* **2013**, *25*, 596−600.
(46) Sun, D.; Yang, Z.; Ren, Z.; Li, H.; Bryce, M. R.; Ma, D.; Yan, S. Oligosiloxane Functionalized with Pendant (1,3-Bis(9-Carbazolyl)-Benzene) (MCP) for Solution-Processed Organic Electronics. *Chem.—Eur J.* **2014**, *20*, 16233−16241.
(47) Penfold, T. J.; Dias, F. B.; Monkman, A. P. The Theory of Thermally Activated Delayed Fluorescence for Organic Light Emitting Diodes. *Chem. Commun.* **2018**, *54*, 3926−3935.
(48) Gibson, J.; Penfold, T. J. Nonadiabatic Coupling Reduces the Activation Energy in Thermally Activated Delayed Fluorescence. *Phys. Chem. Chem. Phys.* **2017**, *19*, 8428−8434.
(49) Graves, D.; Jankus, V.; Dias, F. B.; Monkman, A. Photophysical Investigation of the Thermally Activated Delayed Emission from Films of M-MTDATA:PBD Exciplex. *Adv. Funct. Mater.* **2014**, *24*, 2343−2351.

■ NOTE ADDED AFTER ASAP PUBLICATION

This paper was published on the Web on August 26, 2020, with the incorrect graphic for Figure 7 due to a production error. The corrected version was reposted on August 28, 2020.